Electronic Supplement Material for the publication

Metalloid-doping in SMoSe Janus layers: First-principles study on efficient catalysts for the hydrogen evolution reaction

M. Vallinayagam[a, b], J. Karthikeyan[c], M. Posselt[d], D. Murali[e] and M. Zschornak[f, b]

[a] IEP, TU Bergakademie Freiberg, Akademiestraße 6, 09599 Freiberg, Germany; E-mail: muthu.vallin@gmail.com
[b] Fakultät Maschinenbau/ Energietechnik/Physik, Hochschule für Technik und Wirtschaft Dresden, Friedrich-List-Platz 1, 01069 Dresden
[c] Department of Physics, National Institute of Technology, Durgapur - 713209, West Bengal, India
[d] Helmholtz-Zentrum Dresden-Rossendorf, Institute of Ion Beam Physics and Materials Research, Bautzner Landstraße 400, 01328 Dresden, Germany
[e] Indian Institute of Information Technology Design and Manufacturing, Kurnool-518008, India
[f] IEP, TU Bergakademie Freiberg, Akademiestraße 6, 09599 Freiberg, Germany

1. Optimized structures of X-doped (X = B, Si, Ge) Janus layers

The optimized structures of JLs for each doping site are given for B, Si, and Ge doping in SFig. 1-3.

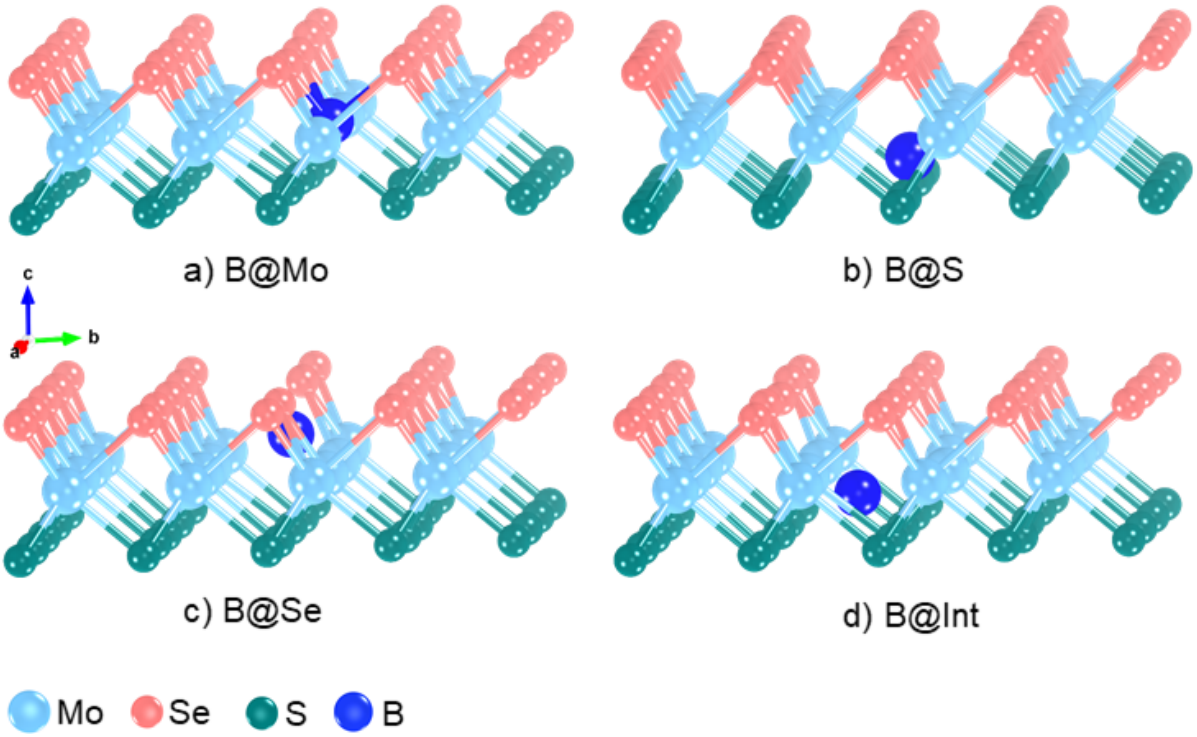

SFig. 1 The relaxed structures of B-doped JLs

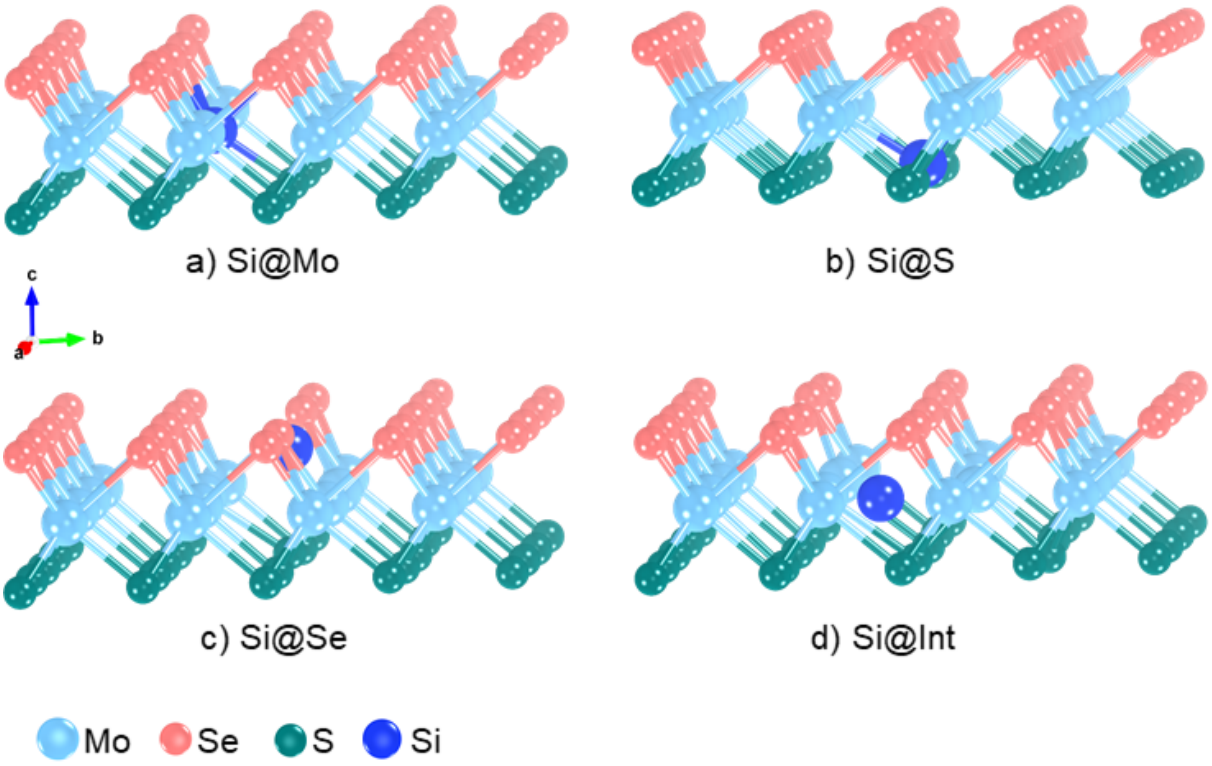

SFig. 2 The relaxed structures of Si-doped JLs

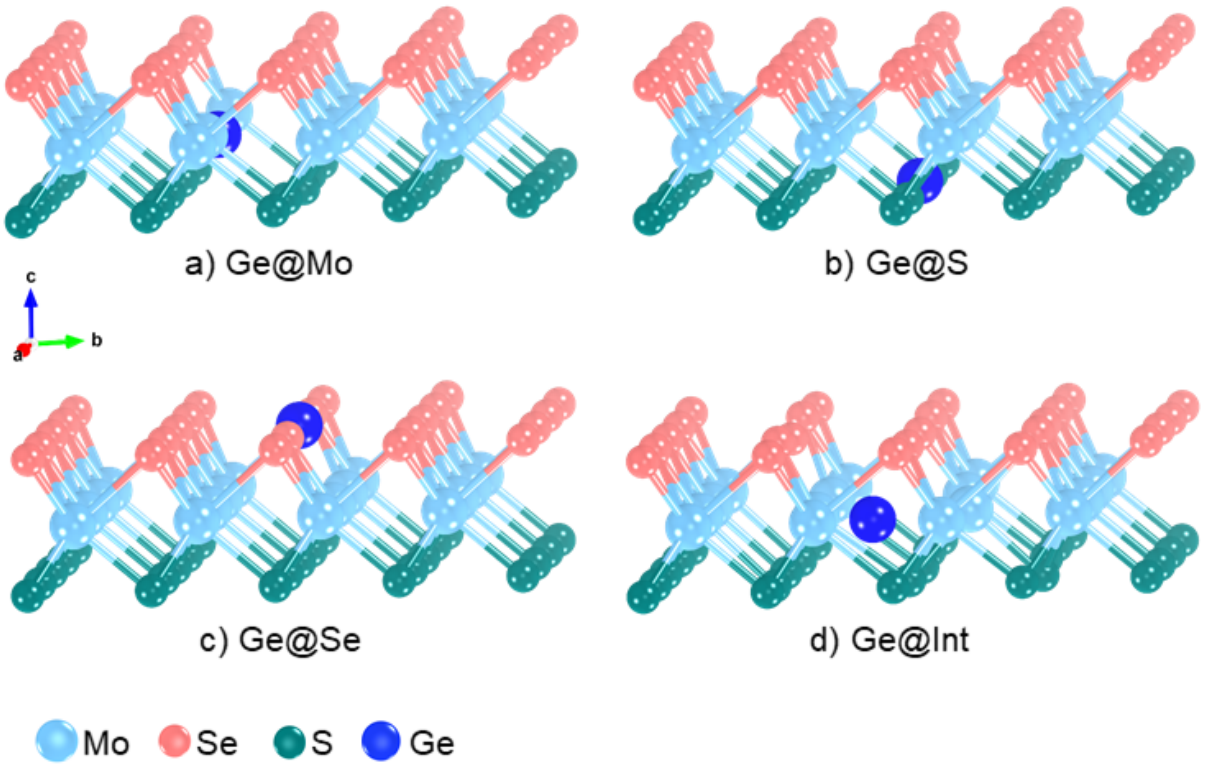

SFig. 3 The relaxed structures of Ge-doped JLs

2. Definition of structural quantities

The structural quantities average bond length (l_{ave})[1], volume (V_{poly})[2], distortion index (d_{idx})[3], and the effective bond number (N_{eff})[1] of the trigonal prismatic coordination containing the dopant X are calculated using the VESTA package[4]. These quantities are defined as follows:

The average bond length is the ratio between the bond length involved in the prismatic coordination and the weight of the bond length and it is calculated as

$$l_{\text{ave}} = \frac{\sum_{i=1} l_i \; w_i}{\sum_{i=1} w_i} = \frac{\sum_{i=1} l_i \exp(1-(l_i/l_{min})^6)}{\sum_{i=1} \exp(1-(l_i/l_{min})^6)} \tag{1}$$

where l_i is the i^{th} bond length from the coordination and w_i ($\exp(1-(l_i/l_{min})^6)$) is the weight of bond length.

The d_{idx} involves l_{ave} as

$$d_{\text{idx}} = \frac{1}{n} \sum_{i=1}^{n} \frac{l_i - l_{ave}}{l_{ave}} \tag{2}$$

where n is the total number of bonds involved in the coordination.

The coordination always involves a central atom in the prismatic polyhedron. Hence the central atom is connected to nearby atoms to complete the coordination. The number of bonds involved in the coordination can be quantified as the effective bond number (N_{eff}) by

$$N_{\text{eff}} = \sum_{i=1} \exp\left(1 - \left(\frac{l_i}{l_{ave}}\right)^6\right) \tag{3}$$

The calculation of polyhedron volume (V_{poly}), *i. e.* the volume of prismatic coordination, is a complicated process and the complete procedure is discussed by Swanson *et al.*[2]. The polyhedron is divided into several tetrahedra and three vectors (denoted by **A**, **B**, **C**) associated with each tetrahedron are used to calculate the V_{poly}. The tetrahedra volume is defined as $1/6\ |\mathbf{A} \cdot (\mathbf{B} \times \mathbf{C})|$ and the volume of tetrahedra is summed up to calculate V_{poly}.

3. H adsorption sites in SMoSe Janus layers

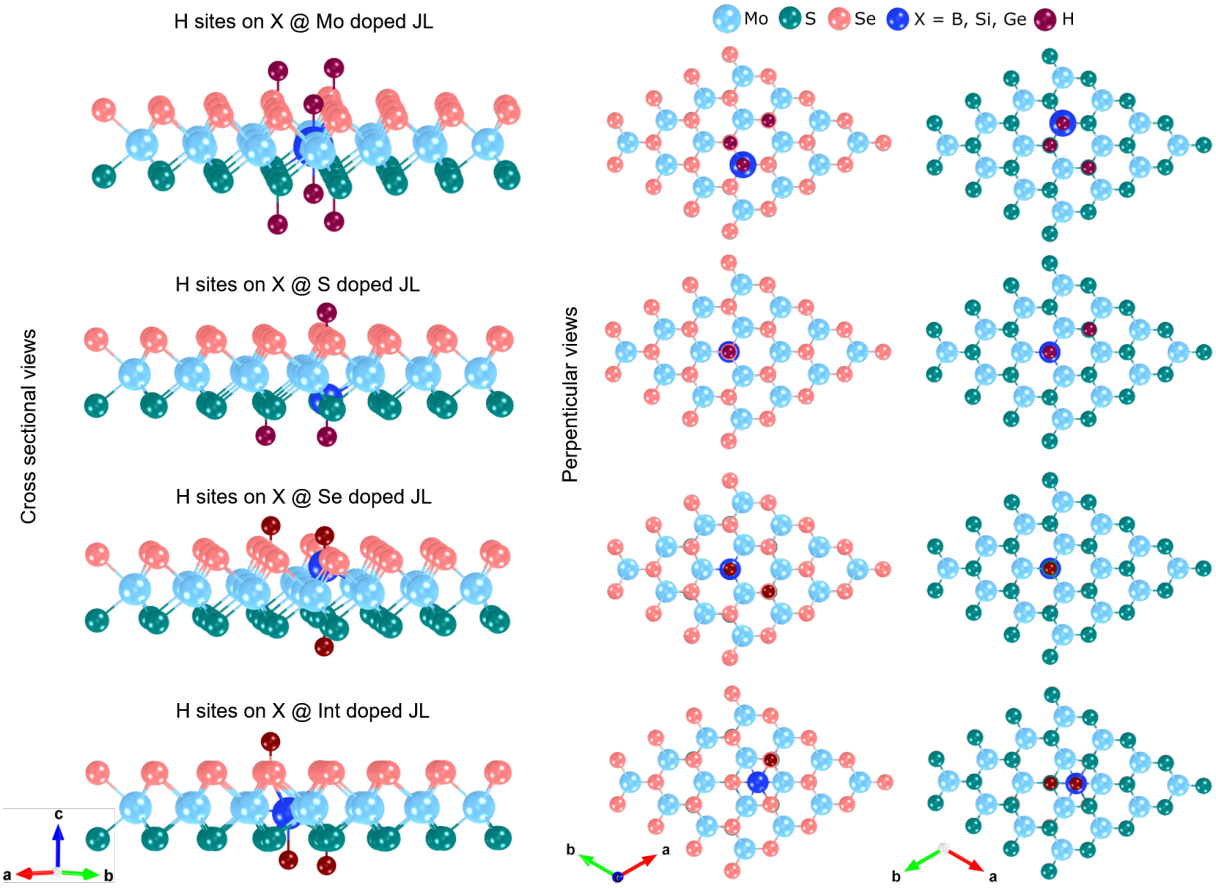

SFig. 4 The feasible sites for H adsorption considered around the dopant in X-doped JLs in cross-sectional and vertical views.

4. Differential Charge Density

The activated sites can be identified for or related to HER activity using either Bader charge analysis or Differential Charge Density (DCD) concepts[5]. To derive explicit results, the atoms with increased or decreased Bader charge will show accumulation or depletion of corresponding charge density. Based on this reasoning, the calculated adsorption enthalpy or Gibbs free energy is supported or evidenced through the calculated Bader charge. Here, we discuss differential charge density exemplarily for Ge-doped SMoSe JLs. The results are shown in SFig. 5. The given plot depicts that irrespective of doping site, the charge accumulation or depletion appears at first nearest neighbor (1NN) atoms. Hence the dopant Ge strongly affects the local charge distribution and the atoms far away are almost not influenced by the new atomistic scenario. Such behavior is highly appreciable to increase the dopant concentration in order to control and optimize the H trapping sites. This interplay between different analysis methods not only enhances the robustness of the findings but also provides a more comprehensive understanding of the intricate interactions within the system under investigation. The found dependence may be further tested with respect to thermodynamic stability of doped layers with higher dopant concentration, which will be a motive for a separate study. Here, we limited ourselves with one dopant atom per 4x4 supercell of SMoSe.

Furthermore, notable characteristics are recognized from the DCD analysis:

1. In the Ge@Mo-doped JL (SFig. 5a-b), there is a pronounced interaction between the dopant Ge and the 1NN Mo and S atoms, surpassing its interaction with Se. Specifically, the charge distribution electron redistribution is markedly concentrated along the Ge-S bond, as illustrated in SFig. 5b. Conversely, the Ge-Se interaction is scarcely perceptible, even when employing an isosurface level as low as 0.001 $e/\AA^3$; reinforcing the assertion that the Ge-S interaction prevails over Ge-Se. Consequently, the 1NN S sites emerge as more optimal for the HER compared to Se. Moreover, Ge exhibits a stronger affinity for interaction with S and Mo, consequently showing limited propensity for bonding with incoming H. This phenomenon is corroborated by the presented Gibbs free energy, depicted in Fig. 6c of the manuscript. The above discussion for Ge@Mo, based on the DCD plots shown in SFig. 5, confirm the Q_i data obtained by Bader analysis given in Table 1 (remarkable and minor electron redistribution to S and Se, respectively, electron depletion at Ge) and, consequently, help to understand the values for the H adsorption enthalpy in Table 2.

2. In the Ge@Se-doped JL (SFig. 5c-d), the dopant interacts prominently with 1NN Mo atoms, and charge electron accumulation occurs between Mo and Ge. This is reflected by the Q_i value in the Bader charge of the Ge atom ($0.047e$, $Q_i = 0.047$, cf. Table 1 in the manuscript). While minor charge redistribution is observed on 1NN Se and S atoms due to lattice distortion. The dopant in the Se plane propagates the distortion up to the S-plane, indicating the strength of the Ge-Mo interaction.

3. The Ge@S doping (SFig. 5e-f) exhibits similarities with the aforementioned scenarios, excluding distortion propagation. Once again, a robust interaction between Ge and Mo is evident. A significant presence of charge redistribution on the S plane is noted found along with almost no contribution from the Se plane at the isosurface level of 0.001 $e/\AA^3$. Notably, the positive Gibbs free energy for HER in Ge@Int doped JL led to its exclusion from the DCD analysis. Since for Ge@Int always a positive H adsorption energy was obtained, this case is not discussed here in terms of DCD analysis.

A similar study is carried out also for the Si@Mo JL. The computed DCD is shown in SFig. 6.

The Bader analysis indicates (Q_i values given in Table 1 of the manuscript) that in this JL the 1NN S atoms hold a higher electron concentration than the remaining S atoms. This is confirmed by the DCD plot. Hence, increased charge accumulation is observed at the 1NN S site, cf. SFig. 6b.

The above results and discussion demonstrate that the Bader charge analysis offers an integral assessment for identifying promising sites in HER studies, whereas the DCD analysis is more informative and comprehensible on a local evaluation (although with a higher computational cost). The more or less one-to-one correspondence between the DCD and Bader charge analysis serves as a crucial validation, affirming the reliability and accuracy of our data presented in the manuscript. This interplay between different analysis methods not only enhances the robustness of the findings but also provides a more comprehensive understanding of the intricate interactions within the system under investigation.

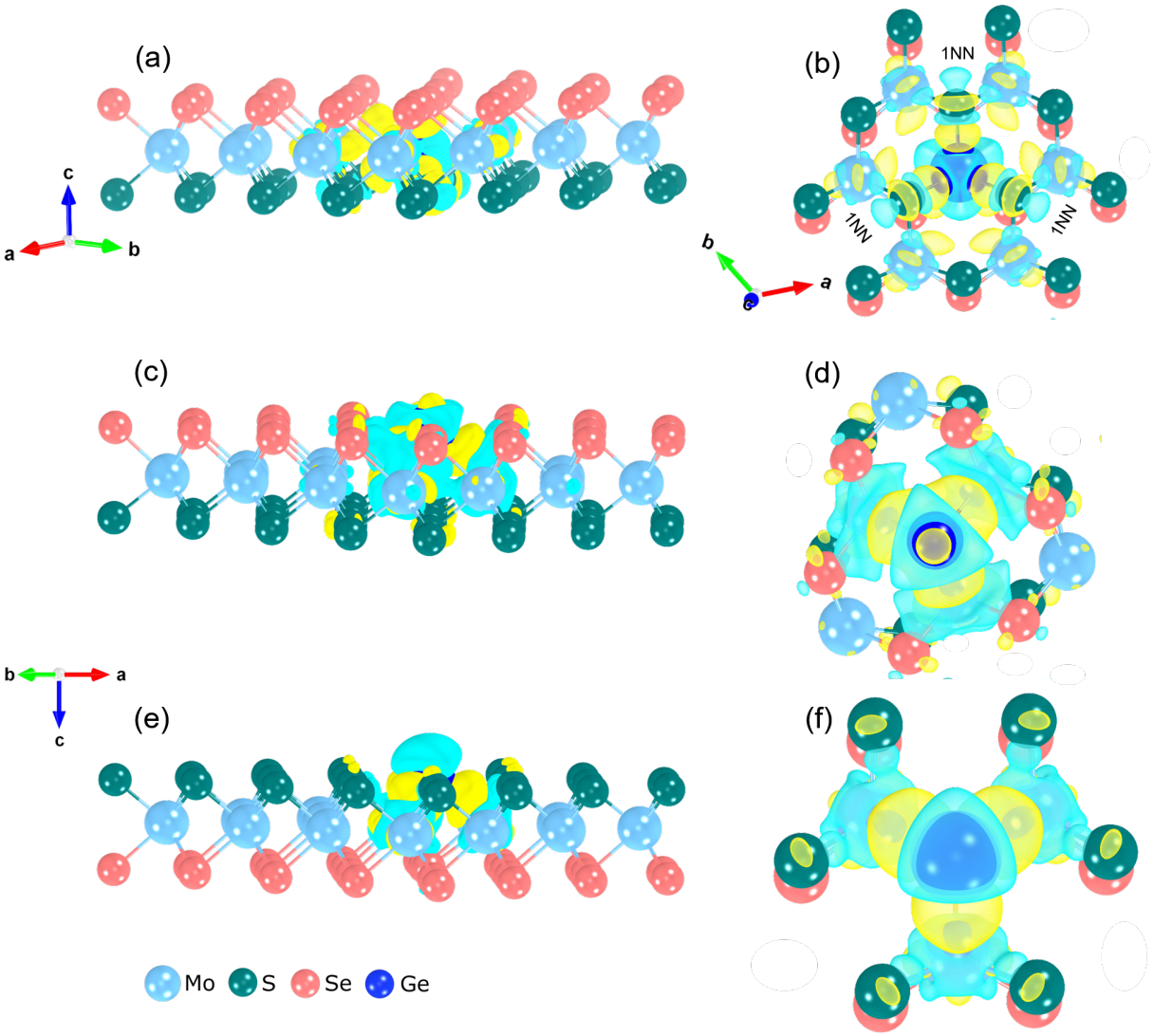

SFig. 5 The differential charge density for (a-b) Ge@Mo- (c-d) Ge@Se- (e-f) Ge@S- doped SMoSe JLs. An isosurface level of 0.001 $e/\mathring{A}^3$ is selected to compare the three dopant sites. The cross sectional views (a, c, e) explicitly depicts that the accumulation or depletion of charge occur at nearby sites to the dopant. In the perpendicular views (b, d, f) a zoomed structural region at the dopant site and its nearest neighbors is shown along with the isosurface. In Ge@Mo JL (b) the first nearest neighbors are denoted by 1NN. The light blue and yellow isosurfaces represent the charge depletion and accumulation with the value of 0.001 $e/\mathring{A}^3$

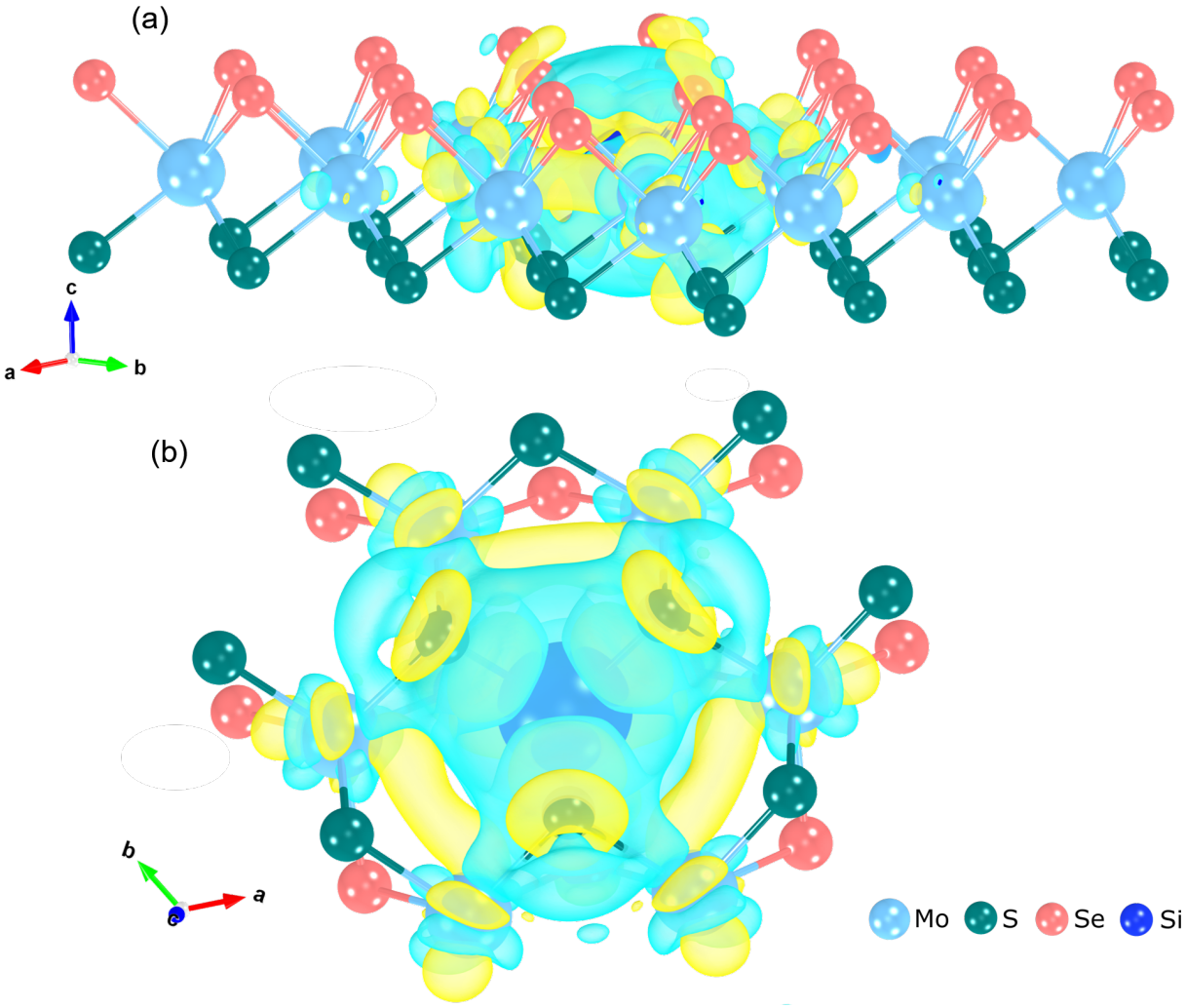

SFig. 6 The differential charge density for Si@Mo-doped SMoSe JLs. Again, an isosurface level of 0.001 $e/\mathring{A}^3$ is used to present charge redistribution. (a) The cross-sectional view explicitly depicts the accumulation and depletion of charge that occurs at nearby sites to the dopant. In the perpendicular view (b) the zoomed part at the dopant site and its nearest neighbors is shown along with the isosurface. The light blue and yellow isosurfaces represent the charge depletion and accumulation with the value of 0.001 $e/\mathring{A}^3$.

5. Data for Gibbs free energy of H adsorption

Table 1 Calculated adsorption energy E_{ad}, zero-point energy of adsorbed H , zero-point energy of H_2 ZPE(H), change in zero-point energy of H ΔZPE and $\Delta G(\mathrm{H}) = E_{ad} - \Delta ZPE - T\Delta S$ tabulated for H adsorption on the pristine SMoSe JL.

H site	E_{ad}	ZPE(H^*)	ZPE(H)	ΔZPE	TΔS	ΔG(H)
pristine SMoSe JL						
H on S	1.673	0.138	0.135	0.004	-0.205	1.882
H on Se	2.189	0.076	0.135	-0.057	-0.205	2.336

Table 2 Calculated adsorption energy E_{ad}, zero-point energy of adsorbed H , zero-point energy of H_2 ZPE(H), change in zero-point energy of H ΔZPE and $\Delta G(\mathrm{H}) = E_{ad} - \Delta ZPE - T\Delta S$ tabulated for H adsorption on the B-doped SMoSe JL.

H site	E_{ad}	ZPE(H^*)	ZPE(H)	ΔZPE	TΔS	ΔG(H)
B@Mo SMoSe JL						
H on S	-2.563	0.306	0.135	0.172	-0.205	-2,186
H on Se	-2.817	0.306	0.135	0.172	-0.205	-2,440
H on B	-1.832	0.290	0.135	0.156	-0.205	-1,471
H on B	-1.680	0.290	0.135	0.156	-0.205	-1,319
B@S SMoSe JL						
H on S	0.322	0.301	0.135	0.166	-0.205	0.693
H on Se	1.095	0.301	0.135	0.166	-0.205	1.467
H on Se	1.112	0.301	0.135	0.166	-0.205	1.483
H on B	-0.373	0.306	0.135	0.172	-0.205	0.003
B@Se SMoSe JL						
H on S	0.211	0.076	0.135	-0.058	-0.205	0.357
H on S	0.213	0.076	0.135	-0.058	-0.205	0.360
H on Se	0.908	0.065	0.135	-0.069	-0.205	1.044
H on B	-0.384	0.308	0.135	0.174	-0.205	-0.005
B@Int SMoSe JL						
H on S	0.552	0.072	0.135	-0.062	-0.205	0.694
H on Se	1.153	0.061	0.135	-0.073	-0.205	1.285
H on B	2.169	0.038	0.135	-0.096	-0.205	2.278

Table 3 Calculated adsorption energy E_{ad}, zero-point energy of adsorbed H , zero-point energy of H_2 ZPE(H), change in zero-point energy of H ΔZPE and $\Delta G(\mathrm{H}) = E_{ad} - \Delta ZPE - T\Delta S$ tabulated for H adsorption on the Si-doped SMoSe JL.

H site	E_{ad}	ZPE(H^*)	ZPE(H)	ΔZPE	TΔS	ΔG(H)
Si@Mo SMoSe JL						
H on S	-0.684	0.154	0.135	0.016	-0.205	-0.463
H on S	0.451	0.152	0.135	0.014	-0.205	0.670
H on Se	-0.480	0.134	0.135	-0.003	-0.205	-0.278
H on Se	1.148	0.271	0.135	0.133	-0.205	1.487
H on Si	1.232	0.116	0.135	-0.022	-0.205	1.415
H on Si	0.712	0.116	0.135	-0.022	-0.205	0.895
Si@S SMoSe JL						
H on S	0.679	0.151	0.135	0.013	-0.205	0.897
H on Se	1.204	0.126	0.135	-0.011	-0.205	1.397
H on Si	-0.776	0.257	0.135	0.119	-0.205	-0.451
Si@Se SMoSe JL						
H on S	0.379	0.149	0.135	0.011	-0.205	0.595
H on Se	1.291	0.134	0.135	-0.004	-0.205	1.492
H on Si	-0.826	0.253	0.135	0.115	-0.205	-0.505
Si@Int SMoSe JL						
H on S	1.458	0.130	0.135	-0.008	-0.205	1.654
H on Se	2.273	0.141	0.135	0.002	-0.205	2.481
H on Si	2.205	0.132	0.135	-0.006	-0.205	2.404

Table 4 Calculated adsorption energy E_{ad}, zero-point energy of adsorbed H , zero-point energy of H_2 ZPE(H), change in zero-point energy of H ΔZPE and $\Delta G(\mathrm{H}) = E_{ad} - \Delta ZPE - T\Delta S$ tabulated for H adsorption on the Ge-doped SMoSe JL.

H site	E_{ad}	ZPE(H^*)	ZPE(H)	ΔZPE	TΔS	ΔG(H)
Ge@Mo SMoSe JL						
H on S	-0.428	0.308	0.135	0.174	-0.205	-0.049
H on Se	-0.224	0.271	0.135	0.136	-0.205	0.116
H on Ge	0.672	0.093	0.135	-0.041	-0.205	0.835
H on Ge	0.884	0.139	0.135	0.005	-0.205	1.094
Ge@S SMoSe JL						
H on S	0.570	0.062	0.135	-0.072	-0,205	0.703
H on Se	1.072	0.070	0.135	-0.063	-0,205	1.213
H on Ge	-0.594	0.252	0.135	0.117	-0,205	-0.271
Ge@Se SMoSe JL						
H on S	0.049	0.066	0.135	-0.068	-0.205	0.186
H on Se	0.976	0.065	0.135	-0.069	-0.205	1.112
H on Ge	-0.881	0.250	0.135	0.115	-0.205	-0.560
Ge@Int SMoSe JL						
H on S	1.211	0.069	0.135	-0.064	-0.205	1.351
H on Se	1.614	0.278	0.135	0.143	-0.205	1.963
H on Ge	2.248	0.051	0.135	-0.082	-0.205	2.370

References

[1] R. Hoppe, *Zeitschrift für Kristallographie - Crystalline Materials*, 1979, **150**, 23–52.

[2] D. K. Swanson and R. C. Peterson, *The Canadian Mineralogist*, 1980, **18**, 153–156.

[3] K. Robinson, G. V. Gibbs and P. H. Ribbe, *Science*, 1971, **172**, 567–570.

[4] K. Momma and F. Izumi, *J. Appl. Crystallogr.*, 2011, **44**, 1272–1276.

[5] N. N. T. Pham, K. H. Kim, B. Han and S. G. Lee, *J. Phys. Chem C*, 2022, **126**, 5863–5872.